Journal of Magnetic Resonance 199 (2009) 117–125

Contents lists available at ScienceDirect

Journal of Magnetic Resonance

journal homepage: www.elsevier.com/locate/jmr

Phase-cycled averaging for the suppression of residual magnetisation in SPI sequences

Joachim B. Kaffanke [a], Tony Stöcker [a], Sandro Romanzetti [a], Thomas Dierkes [b], Martin O. Leach [c], N. Jon Shah [a,d,*]

[a] Institute of Neuroscience and Medicine 4 - Medicine, Forschungszentrum Jülich GmbH 52425 Jülich, Germany
[b] Institute for Biomagnetism and Biosignal Analysis, University of Münster, 48149 Münster, Germany
[c] Cancer Research UK Clinical Magnetic Resonance Research Group, The Institute of Cancer Research and The Royal Marsden NHS Foundation Trust, Downs Road, Sutton, Surrey SM2 5PT, UK
[d] Department of Neurology, University Hospital Aachen, RWTH Aachen University, 52074 Aachen, Germany

ARTICLE INFO

Article history:
Received 27 March 2008
Revised 5 November 2008
Available online 6 December 2008

Keywords:
MRI
Single point imaging
SPRITE
SPI
Residual magnetisation
Artefacts
Phase cycling
Phase graphs
Extended phase graphs
Extended phase encode graphs
EPEG
Phase cycling filter
Phase-cycled averaging
FID
Spin echo
Stimulated echo

ABSTRACT

Residual magnetisation is one of the major sources of artefacts in single point imaging sequences with short repetition times. The unwanted signal is caused by non-dephased transverse magnetisation excited in preceding acquisition cycles. Therefore, the problem emerges mainly around the centre of *k*-space and has been solved in the past by additional spoiling gradients. In this work, unwanted residual magnetisation acquired with the SPRITE sequence was investigated and a new method for the suppression of residual magnetisation is presented. It is shown that residual magnetisation experiences a different phase encoding leading to residual images with a different FOV. A phase cycling filter is able to eliminate the unwanted signal. Furthermore, a description of all signal components that occur is presented using an operator notation. The notation is new in this field with respect to its completeness. That is, the signal description is based on an understanding of single point imaging sequences, such as SPRITE, by the use of an extended phase encode graph.

A prominent *in vivo* example is that of sodium imaging in biological tissue where transverse relaxation times are such that unwanted coherences can occur and therefore residual magnetisation becomes a significant problem. For instance, sodium in biological tissue has two transverse relaxation times of approximately 3 ms and 15 ms at 4 T and this can result in significant artefacts if the encoding time is short and TR $\ll$ 3 ms.

1. Introduction

Single point imaging sequences (SPI) as introduced by Emid and Creyghton [1] are purely phase encoding sequences. After settling of 3D phase encode gradients, a broadband radio frequency pulse is applied for excitation of the whole volume and following a fixed encoding time, which is only restricted by the maximum gradient strength and the ring down time of the radio frequency coil, a single *k*-space point is acquired. After data acquisition the gradients are ramped down to zero for the rest of the repetition time to minimise the gradient duty cycle. SPI sequences are mainly suited for acquisition of fast relaxing nuclei since no gradient switching is needed between excitation and data acquisition.

The virtue of the SPRITE sequence (Single Point Ramped Imaging with T_1 Enhancement) developed by Balcom et al. [2] lies in the use of gradient ramps for the acquisition of an entire line of *k*-space points to avoid extensive switching of the phase encoding gradients thus reducing the gradient noise. This also provides the opportunity to use short repetition times, *TR*, for the gradient steps. This, however, can be problematic if *TR* is on the order of the transverse relaxation time, T_2^*. Assuming a SPRITE acquisition in the absence of all gradients, that is a train of RF pulses interspersed with the acquisition of single points, transverse magnetisation would be left in each acquisition window from the preceding RF pulses. This problem is reduced by self-spoiling phase encode gradients and hence not present in the outer parts of *k*-space. However, residual magnetisation influences the signal around the centre of *k*-space

* Corresponding author. Address: Institute of Neuroscience and Biophysics 3 - Medicine, Forschungszentrum Jülich GmbH 52425 Jülich, Germany. Fax: +49 2461 61 8294.
E-mail address: n.j.shah@fz-juelich.de (N.J. Shah).

1090-7807/$ - see front matter © 2009 Published by Elsevier Inc.
doi:10.1016/j.jmr.2008.11.018

and can lead to an overall intensity increase or decrease as well as the typical 'cloud' artefacts.

In an earlier work from Kennedy et al. [3], the problem of residual magnetisation in SPRITE imaging sequences has already been discussed. The phenomenon was thought to be mainly due to spin and stimulated echo effects (Hahn [4]). Kennedy et al. report about SPRITE experiments with a manganese-doped gel phantom. They used additional spoiler gradients around the *k*-space centre to dephase the unwanted signal. The ratio of spin echo and stimulated echo signal to the FID signal is a function of $\sin^2(\alpha/2)$ and $\sin^2(\alpha)$, respectively, (Liang and Lauterbur [5]). The echo effects are consequently negligible for small flip angles $a \ll 90^\circ$ which is certainly the case for typical SPRITE sequences where $\alpha < 10^\circ$.

In the past SPI techniques such as SPRITE were mainly used for solid state NMR. Here, transverse relaxation times are very short whereas longitudinal relaxation is typically long. A sufficiently long repetition time, *TR*, may be chosen to avoid artefacts, since there are no severe limitations in acquisition time. Thus, for solid-state applications a suppression of residual magnetisation was not generally needed. For applications concerning biological tissue where transverse relaxation times are longer and for *in vivo* experiments, with naturally restricted acquisition times, the residual magnetisation becomes a significant problem. For instance, sodium in biological tissue has two transverse relaxation times of approximately 3 ms and 15 ms at 4 T and this can result in significant artefacts if the encoding time is short and TR $\ll$ 3 ms. T_2^* relaxation time mapping of fast-relaxing nuclei in biological tissue is the future potential of SPRITE with the extension to multiple point acquisition (*m*-SPRITE) [6,7]. The results presented here are focused on single point acquisition SPRITE for simplicity but can be easily extended and applied to *m*-SPRITE sequences.

Normal cell physiology relies upon numerous factors with one of the most important of these being the presence of highly regulated sodium concentrations in the intra-cellular and extra-cellular compartments. In healthy tissue, sodium is present in concentrations of about 10 mM intracellular and 150 mM extracellular. Since the average tissue sodium concentration measured by sodium MRI correlates with a variety of diseases, it can be regarded as an ideal means to monitor pathologies *in vivo*. In such circumstances, artefact-free and quantitative images of sodium could prove to be of great value. Therefore, there is a strong motivation for the pursuit of quantitative ^{23}Na MRI whereby artefact suppression is clearly a prerequisite.

In this article, it is shown that a description using *k*-space subsets of different phase encodings, Δk, is appropriate for viewing residual magnetisation, leading to a superposition of images with different FOVs. These artefacts result from different signal components excited by the series of RF pulses in SPRITE. The signal components are described with the use of an extended phase encode graph (EPEG) theory. An algebraic formulation is given analogous to the partitioning of magnetisation presented earlier in the work of Kaiser et al. [8].

The residual magnetisation can be efficiently averaged to zero by use of a phase cycling filter. This has been implemented here by the acquisition of N SPRITE scans with different phase cycling steps for each acquisition. Each phase cycling step has a fixed angle between 0 and 2π between consecutive scan. Only residual signal components experience phase rotation and the average of those components is zero. Thus, residual magnetisation is suppressed.

2. Theory

Any SPI sequence and especially SPRITE can be decomposed into a series of short broadband RF excitation pulses and propagators which describe the signal evolution between the pulses. The RF pulses are defined by the flip angle α. The flip angle may be spatially dependent because of B_1 inhomogeneities and off-resonance effects may play a role. The propagators are given by the longitudinal and transverse relaxation times, T_1 and T_2, and all variations of the precession frequency, ω. The frequency of the spin system is investigated with respect to the local oscillator of the NMR spectrometer. The latter should be on resonance at the Larmor precession frequency, $\omega_0 = \gamma B_0$, depending on the gyromagnetic ratio of the nucleus, γ, and the static magnetic field, B_0. Field inhomogeneities, susceptibility gradients, chemical shifts as well as the phase encode gradients together with concomitant gradient fields change the phase of the magnetisation and contribute to the propagator.

2.1. Partitioning of magnetisation

In this section, a complete operator formalism is introduced to describe the partitioning of magnetisation similar to Kaiser et al. [8]. This partitioning of magnetisation was first time used in the work of Woessner [9]. Here, it will lead to a description of superimposing *k*-spaces all experiencing different signal evolution and phase encoding.

In order to derive simple solutions for the Bloch equations all equations are given in the rotating coordinate system with Larmor frequency ω_0. In a vector description the magnetisation is given by the transverse components, M_x, M_y, and the longitudinal magnetisation, M_z. With use of the complex notations $M_{xy} = M_x + iM_y$ and $M_{xy}^* = M_x - iM_y$ for transverse magnetisation and its complex conjugate, respectively, a rotation by an α-pulse can be expressed by three terms for transverse and longitudinal polarisation each. Here, the '+' and '−' super-scripts indicate post- and pre-pulse magnetisation, respectively.

$$^{+}M_{xy} = {}^{-}M_{xy}\cos^2\frac{\alpha}{2} - {}^{-}M_{xy}^*\sin^2\frac{\alpha}{2} - M_z\sin\alpha \tag{1a}$$

$$^{+}M_z = {}^{-}M_z\cos\alpha + \frac{1}{2}({}^{-}M_{xy} + {}^{-}M_{xy}^*)\sin\alpha \tag{1b}$$

Thus, each pulse subdivides the magnetisation components into either longitudinal or transverse magnetisation with or without phase inversion. After excitation the transverse magnetisation experiences phase evolution under the influence of the phase changing effects of the propagator as mentioned above. Since the longitudinal magnetisation shows phase memory for components excited from the transverse polarisation, M_z also has a phase which is unchanged by the propagator. This leads to six possible branches with separate phase evolution and specific phase coherence (see Fig. 1).

Consequently, the RF pulse train gives rise to a tree of coherence pathways. Between the pulses the transverse magnetisation is phase encoded by the phase encode gradients. Every coherence pathway experiences a different phase encoding which accumulates during the RF pulse train. The amplitude of the phase encode gradients between RF pulses defines a velocity of phase rotation. By integration of the phase encode gradients over time a movement through *k*-space is given. This can be depicted by straight lines between RF pulses where the slope is proportional to the phase encode gradient amplitude. These phase encode graphs are extended by the magnetisation amplitudes excited by the RF pulses. Thus, the spin dynamics of SPI sequences are described by an extended phase encode graph (EPEG) that is shown in Fig. 2.

In order to derive a complete representation of all signal components, an operator notation may be used. The excitation pulses, *P*, rotate the magnetisation, *M*, around the axis of polarisation of the RF field which shall define the *y*-axis. The orientation of the polarisation axis is fixed to the rotating frame coordinate system which is given by the phase of the local oscillator producing the radio frequency. For the propagator an operator, *U*, is used that does not commute with the RF pulse operator, *P*.

Indices $l = -1,0,1$ and $m = 0,1$ are used to classify every possible coherence pathway. The polarisation index, *m*, differentiates between polarisations of longitudinal magnetisation with $m = 0$ and

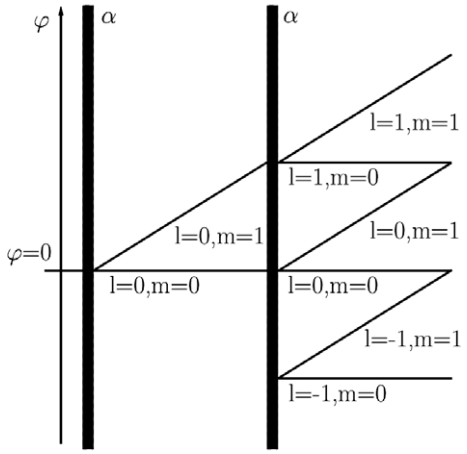

Fig. 1. The possible signal coherences that are excited by successive RF pulses subdivide in three transverse and three longitudinal magnetisations (tilted and horizontal lines, respectively). Longitudinal magnetisation subdivides into two pathways of longitudinal and transverse polarisation. Transverse magnetisation subdivides into the two polarisations and additionally experiences phase inversion. The slope of the transverse magnetisation pathways denotes the phase evolution. Each pathway is characterised by the pathway selection indices *l* and *m*. The integration of the phase distribution in space leads to *k*-space encoding (see Fig. 2).

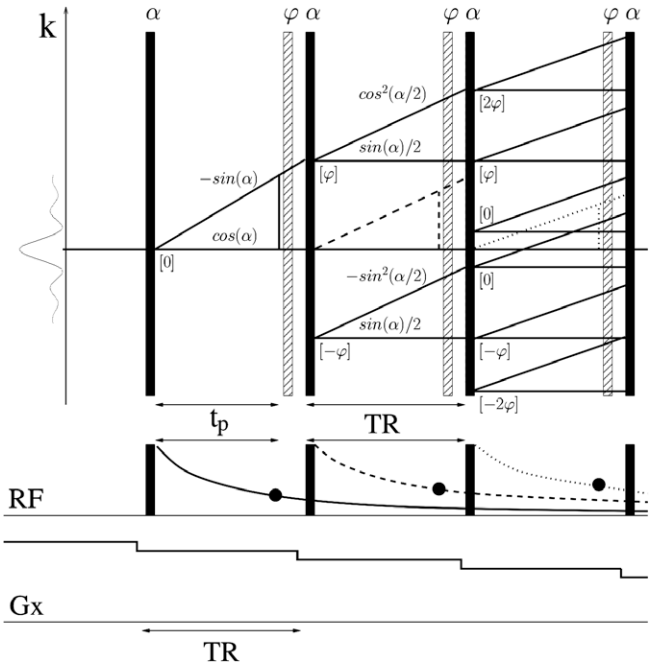

Fig. 2. (bottom) SPRITE sequence diagram showing gradient ramp of the primary phase encode gradient, Gx, with repetition time, *TR*, and the RF pulse train with the first three excitations. Each excitation pulse gives rise to an individual FID with individual phase encoding. Three FIDs are plotted with solid, dashed and dotted line. The FIDs interfere at acquisition time, t_p, following each excitation, (top) The extended phase encode graph (EPEG) describes all signal pathways which are excited by RF pulses with flip angle α (solid vertical bars). Horizontal lines represent longitudinal and tilted lines denote transverse magnetisation. The slope of transverse magnetisation depends on the strength of the phase encode gradients. Thus, the distance to the state of longitudinal equilibrium magnetisation is a measure for the phase encoding and therefore the *k*-space coordinate. For the first FID (solid line) excited by the first RF pulse all following transitions are plotted to the third order whereas for the other two first order FIDs (dashed and solid lines), the higher order signal pathways are not shown. The phase encode graph is extended by signal magnitudes depending on the flip angle α. The effect of the phase cycling depends on the signal order and is calculated with respect to the first RF pulse and the excited first order FID (solid line). The total phase of the signal pathways that is introduced by the phase rotations with phase angle φ (dashed bar) is given in squared brackets. The phase rotation is applied after signal acquisition and longitudinal magnetisation is unaffected. Signals with a total phase of zero are not suppressed by the phase-cycled averaging.

transverse magnetisation with $m = 1$. The pre-pulse history of the magnetisation needs to be defined by the transition index l to indicate the type of transition. For $l = 0$ the magnetisation had longitudinal polarisation whilst $l = -1,1$ denotes transverse polarised pre-pulse magnetisation. A phase inversion of transverse magnetisation is indicated by $l = -l$. The RF pulse operators, $P_{n,l,m}$, are counted with $n = 1,2,\ldots$ and the subscripts l,m specifying one of six possible transitions.

The flip angle, α, may be spatially variable thereby taking account of B_1 inhomogeneities. These effects shall be neglected here. Therefore, the abbreviation $\alpha_n \equiv \alpha_n(\vec{r})$ allows one to write the RF pulse propagator as a function of the flip angles alone.

$$P_{n,l,m} \equiv P_{n,l,m}(\alpha_n) \equiv P_{n,l,m}(\alpha_n(\vec{r})) \tag{2}$$

By the use of the transition vector, $\vec{l}$, and the polarisation vector, $\vec{m}$, with components, l_n,m_n, every possible pathway is uniquely defined. Together, they are therefore called the pathway selection vectors. According to these definitions, the following selection rule has to be applied for the choice of the pathway selection indices l_n,m_n:

$$|l_n| = m_{n-1} \tag{3}$$

with the initial condition that $l_0 = m_0 = 0$.

The pathway selection vectors $\vec{l},\vec{m}$ are now used to indicate pre- and post-pulse magnetisations ${}^{-}M^{\vec{l},\vec{m}}_{n-1,l,m}$ and ${}^{+}M^{\vec{l},\vec{m}}_{n,l,m}$, respectively, for specific coherence pathways. Here, the subindices l,m indicate the last pulse transitions l_n,m_n of the pathway selection vectors $\vec{l},\vec{m}$. The magnetisation is a function of spatial position. For simplicity, the abbreviation $M_{n,l,m} \equiv M^{\vec{l},\vec{m}}_{n,l,m}(\vec{r})$ is used as long as spatial encoding and a specific coherence pathway are not under consideration. With this notation the six possible transitions can be written as:

$${}^{+}M_{n,0,0} = P_{n,0,0}\,{}^{-}M_{n-1,l,0} = \cos\alpha_n \cdot {}^{-}M_{n-1,l,0} \tag{4a}$$

$${}^{+}M_{n,0,1} = P_{n,0,1}\,{}^{-}M_{n-1,l,0} = -\sin\alpha_n \cdot {}^{-}M_{n-1,l,0} \tag{4b}$$

$${}^{+}M_{n,-1,0} = P_{n,-1,0}\,{}^{-}M_{n-1,l,1} = \frac{1}{2}\sin\alpha_n \cdot {}^{-}M_{n-1,l,1} \tag{4c}$$

$${}^{+}M_{n,-1,0} = P_{n,-1,0}\,{}^{-}M_{n-1,l,1} = \frac{1}{2}\sin\alpha_n \cdot ({}^{-}M_{n-1,l,1})^{*} \tag{4d}$$

$${}^{+}M_{n,1,1} = P_{n,1,1}\,{}^{-}M_{n-1,l,1} = \cos^2\frac{\alpha_n}{2} \cdot {}^{-}M_{n-1,l,1} \tag{4e}$$

$${}^{+}M_{n,-1,1} = P_{n,-1,1}\,{}^{-}M_{n-1,l,1} = -\sin^2\frac{\alpha_n}{2} \cdot ({}^{-}M_{n-1,l,1})^{*} \tag{4f}$$

where the operator $P_{n,l,m}$ performs a complex conjugation for $l = -1$ and is therefore not linear.

Between the RF pulses, that are applied with repetition time *TR*, the magnetisation experiences relaxation and dephasing. These processes are commutative and can be combined in a single operator, $U_{n,l,m}$, describing the propagation processes of the magnetisation. The phase evolution depends on the field at the spatial position, $\vec{r}$, as well as the gradient field strength with respect to the sequence timing. The timing is denoted by the absolute time of RF pulse application, τ_n, with $\tau_0 = 0$ for the first RF pulse and *TR*. Furthermore, a rotation of magnetisation phases with phase angle, φ_n, is taken into account. Signal propagation may then be written as:

$${}^{-}M_{n,l,m} = U_{n,l,m}(TR,\tau_n,\varphi_n,\vec{r})\,{}^{+}M_{n,l,m} \tag{5}$$

where the propagator is composed of three terms describing the dephasing by gradients and other off-resonance terms, $G_{n,l,m}$, transverse and longitudinal relaxation, $T_{n,l,m}$, and the phase rotation, $R_{n,l,m}$.

$$U_{n,l,m}(\Delta t,\tau_n,\varphi_n,\vec{r}) = R_{n,l,m}(\varphi_n)\cdot T_{n,l,m}(\Delta t,\vec{r})\cdot G_{n,l,m}(\Delta t,\tau_n,\vec{r}) \tag{6}$$

An arbitrary encoding interval, Δt, is used to take signal samples at any time point. Quadrupolar interactions are neglected in this context but could also be introduced. It is noted that Eq. (6) is only formal and cannot be calculated by simple multiplication because of non-linearity.

The phase rotation $R_{n,l,m}$ is only applied to transverse magnetisation $M^{\vec{l},\vec{m}}_{n,l,1}(\vec{r})$ with $m = 1$ whereas longitudinal magnetisation $M^{\vec{l},\vec{m}}_{n,l,0}(\vec{r})$ with $m = 0$ has phase memory.

$$R_{n,l,m}(\varphi_n) = \begin{cases} \exp(i\varphi_n) & \text{for } m = 1 \\ 1 & \text{for } m = 0 \end{cases} \tag{7}$$

The relaxation is governed by the longitudinal and transverse relaxation times, T_1 and T_2, respectively, leading to relaxation operators:

$$T_{n,l,1}(\Delta t, \vec{r}) = \exp(-\Delta t/T_2(\vec{r})) \tag{8a}$$

$$T_{n,l,0}(\Delta t, \vec{r}) = \exp(-\Delta t/T_1(\vec{r})); \quad |\vec{m}| \neq 0 \tag{8b}$$

The relaxation operator, $T_{n,l,m}$, takes a non-linear form for the completely dephased longitudinal magnetisation, ${}^{+}M_{n,0,0}$, that did not experience transverse evolution and propagates to equilibrium magnetisation $M_0(\vec{r})$.

$$T_{n,0,0}(\Delta t, \vec{r})\,{}^{+}M_{n,0,0}(\vec{r}) = \exp(-\Delta t/T_1(\vec{r})) \cdot {}^{+}M_{n,0,0}(\vec{r}) + (1 - \exp(-\Delta t/T_1(\vec{r}))) \cdot M_0(\vec{r}); |\vec{m}| = 0 \tag{8c}$$

The dephasing of transverse magnetisation is described with the operator $G_{n,l,m}$. These processes are caused by any kind of off-resonances from the Larmor frequency, ω_0. The variation of precession frequency is temporally and spatially dependent and can be divided in to two terms for phase encode gradients, $\vec{G}(t)$, and residual off-resonant frequencies, $\delta\omega(\vec{r}, t)$.

$$\Delta\omega(\vec{r}, t) = \gamma\vec{G}(t)\vec{r} + \delta\omega(\vec{r}, t) \tag{9}$$

The dephasing operator is defined as a phase term with an integral of the off-resonances over time. For longitudinal magnetisation, the operator is one.

$$G_{n,l,m}(\Delta t, \tau_n, \vec{r}) = \begin{cases} \exp(i\int_{\tau_n}^{\Delta t+\tau_n} \Delta\omega(\vec{r}, t)\mathrm{d}t) & \text{for } m = 1 \\ 1 & \text{for } m = 0 \end{cases} \tag{10}$$

The residual off-resonances may be caused by B_o field inhomogeneities, susceptibility gradients, chemical shifts and concomitant gradient fields. These effects are neglected in the following and therefore the abbreviation used is as follows:

$$\Delta\omega(\vec{r}, t) = \gamma\vec{G}(t)\vec{r} \tag{11}$$

Thus, the operator $G_{n,l,1}$ now takes over the usual form of the Fourier kernel for k-space encoding. The repetitive use of this operator over intervals Δt and TR explains the different FOVs of residual images (see below) which are the main artefacts in SPRITE imaging of biological tissue.

The magnetisation, $M^{\vec{l},\vec{m}}_{n,l,m}(\vec{r})$, can now easily be written as an operator product of pulses, $P_{n,l,m}$, and propagators, $U_{n,l,m}$, for specific pathway selection vectors, $\vec{l}, \vec{m}$, that is applied to the equilibrium magnetisation, $M_0\vec{r}$.

$$M^{\vec{l},\vec{m}}_{n,l,m}(\Delta t_n, \vec{r}) = \prod_{i=1,..,n} [U_{i,l,m}(\Delta t_i, \tau_i, \varphi_i, \vec{r}) \bullet P_{i,l,m}(\alpha_i)] M_0(\vec{r}) \tag{12}$$

The '•' indicates that the operators do not commute. After n RF pulses the MR signal, S_n, is acquired with a phase encoding time t_p such that $\Delta t_n \equiv t_p$ and $\Delta t_i \equiv TR$ for $i = 1,\ldots,n-1$. The signal is composed of all coherences of the magnetisation given by pathway selection vectors, $\vec{l}, \vec{m}$. Thus, the MR signal from an infinitesimal voxel at position $\vec{r}$ calculates as a sum of all magnetisations, $M^{\vec{l},\vec{m}}_{n,l,m}(\vec{r})$, over all pathway selection vectors, $\vec{l}, \vec{m}$. Given that the signal is acquired in the transverse plane, the last polarisation index has to be $m = 1$.

$$\begin{aligned} S_n(t_p, \vec{r}) &= \sum_{\substack{\vec{l},\vec{m} \\ m_n=1}} U_{n,l,1}(t_p, \tau_n, \varphi_n, \vec{r})\,{}^{+}M^{\vec{l},\vec{m}}_{n,l,1}(\vec{r}) \\ &= \sum_{\substack{\vec{l},\vec{m} \\ m_n=1}} T_{n,l,1}(t_p) \cdot G_{n,l,1}(t_p, \tau_n, \vec{r})\,{}^{+}M^{\vec{l},\vec{m}}_{n,l,1}(\vec{r}) \\ &= \sum_{\substack{\vec{l},\vec{m} \\ m_n=1}} \prod_{i=1..,n} [U_{i,l,m}(\Delta t_i, \tau_i, \varphi_i, \vec{r}) \bullet P_{i,l,m}(\alpha_i)] M_0(\vec{r}) \end{aligned} \tag{13}$$

Finally, the total k-space signal, $\widehat{S}_n$, is given by the integral over the whole space, V.

$$\begin{aligned} \widehat{S}_n(t_p) &= \int_V \sum_{\substack{\vec{l},\vec{m} \\ m_n=1}} S^{\vec{l},\vec{m}}_{n,l,1}(t_p, \vec{r})\mathrm{d}\vec{r} \\ &= \int_V \sum_{\substack{\vec{l},\vec{m} \\ m_n=1}} \prod_{i=1..,n} [U_{i,l,m}(\Delta t_i, \tau_i, \varphi_i, \vec{r}) \bullet P_{i,l,m}(\alpha_i)] M_0(\vec{r})\mathrm{d}\vec{r} \end{aligned} \tag{14}$$

In single point imaging one is only interested in acquiring pure FID signals excited from longitudinal magnetisation without prior phase information. These are transitions of the completely dephased longitudinal magnetisation, ${}^{-}M^{\vec{0},\vec{0}}_{n,0,0}$, to transverse magnetisation, ${}^{+}M^{\vec{0},\vec{m}}_{n,0,1}$, with $\vec{l} = 0$ and $m = 1$.

Generally, let j define the signal order of a coherent pathway, which means that no FID was present prior to the last j pulses. Thus, along these pathways the magnetisation remained along the z-axis followed by a transition to transverse magnetisation, i.e.:

$$\begin{aligned} &m_k = 0 \;\forall \quad k \leqslant n - j \\ &m_{n-j+1} = 1 \end{aligned} \tag{15}$$

These subsets of pathways are subject to phase-encoding and relaxation by T_1 and T_2 depending on $|l_n|$ during the sequence of the last j TR intervals $n - j + 1,\ldots,n$.

Signals with signal order $j = 1$ can be defined as first order FIDs. After the following RF pulse, together with a next first order FID, a second order FID as well as a phase inverted spin-echo signal are acquired (see Fig. 2). Spin-echo signals are regarded in this context as second order signals. After the third pulse, third order signals can also be acquired including a stimulated echo signal.

The SPRITE dataset can be understood as a superposition of different k-spaces with different signal order j and different encoding times t_j. Thus, the magnetisation of signal order j with pathway selection vectors $\vec{l}, \vec{m}$ for every nth RF pulse can be written as:

$$M^{\vec{l},\vec{m}}_{n,j,l,m}(\Delta t_n, \vec{r}) = \prod_{i=n-j+1,..,n} [U_{i,l,m}(\Delta t_i, \tau_i, \varphi_i, \vec{r}) \bullet P_{i,l,m}(\alpha_i)] M^{\vec{0},\vec{0}}_{n-j,0,0,0}(\vec{r}) \tag{16}$$

with $m_{n-j+1} = 1$ such that $P_{n-j+1,l,m}(\alpha_{n-j+1}) \equiv P_{n-j+1,0,1}(\alpha_{n-j+1})$.

Each of these magnetisations, which are a function of the signal order, j, and pathway selection vectors, $\vec{l}, \vec{m}$, form a separate sub k-space, $\widehat{S}^{\vec{l},\vec{m}}_j$, which is given by integration over space. This can be written as:

$$\begin{aligned} \widehat{S}^{\vec{l},\vec{m}}_j(n, t_p) &\equiv \widehat{S}^{\vec{l},\vec{m}}_{n,j}(t_p) \\ &= \int_V \prod_{i=n-j+1,..,n} [U_{i,l,m}(\Delta t_i, \tau_i, \varphi_i, \vec{r}) \bullet P_{i,l,m}(\alpha_i)] M^{\vec{0},\vec{0}}_{n-j,0,0,0}(\vec{r})\mathrm{d}\vec{r} \end{aligned} \tag{17}$$

with $m_{n-j+1} = 1$ and $m_n = 1$ such that $P_{n-j+1,l,m}(\alpha_{n-j+1}) \equiv P_{n-j+1,0,1}(\alpha_{n-j+1})$ and $P_{n,l,m}(\alpha_n) \equiv P_{n,l,1}(\alpha_n)$. Of course, every coherence pathway results in a different phase encoding by integration over the phase encode operator G. Therefore, only the first order FID

results in the artefact-free image whereas all higher order signals lead to residual images and appear as artefacts.

2.2. Phase cycle filter

This section constructs filters to eliminate signal contributions of unwanted signal order j. A filter for residual signals can be created by phase rotation with the operator $R_{n,l,1}(\varphi_n) = e^{i\varphi_n}$. The phase rotation of the spin system is meant to be relative to the phase of the local oscillator of the NMR spectrometer. This is technically implemented by setting the frequency of the local oscillator for a short time τ off-resonant with an offset frequency $\Delta\omega$ such that $\varphi = \tau \cdot \Delta\omega$ This is done following each acquisition and before the next RF pulse and thus, the signal acquisition of the first order FID is always phase locked to the local oscillator. Therefore, a phase shift of the oscillator is equivalent to a rotation of the spin system in the rotating coordinate system of the radio frequency. Since the completely dephased longitudinal magnetisation $M^{\vec{0},\vec{0}}_{n-j,0,0,0}(\vec{r})$ has no phase properties, the phase rotation is counted now by the index j of the signal order.

Under the influence of the RF pulses the phase of the magnetisation is inverted for transitions with transition index $l = -1$ whereas the phase is preserved for $l = 1$ and $l = 0$. This can be expressed by taking the power l^l. Additionally, for longitudinal magnetisation with $m = 0$ the phase is unchanged because of phase memory. With phase rotations of rotation angle φ_j the accumulated phase, θ_j, is calculated by a series with a recursion formula given by:

$$\theta_j = (\theta_{j-1} + m_{j-1}\varphi_{j-1}) \cdot (l_j)^{l_j}; \quad \theta_1 = 0 \tag{18}$$

Depending on the transition vector, $\vec{l}$, it follows that:

$$\theta^{\vec{l}}_j = \sum_{k=1}^{j-1} m_k \varphi_k \prod_{i=k+1}^{j} (l_i)^{l_i}; \quad \theta^0_1 = 0 \tag{19}$$

For any signal acquired with order, j, the phases, φ_1 to φ_{j-1}, from preceding propagators are relevant, but only transverse magnetisation with $m = 1$ experiences a phase change. Each of these phases, φ_k, may experience phase inversion by the following RF pulses with transition indices, l_{k+1} to l_j. The special case $\theta^0_1 = 0$ expresses the phase lock between RF pulse and the following acquisition.

By implementing a phase cycling with constant phase $\varphi_k \equiv \varphi$ a filter for residual magnetisation can be constructed. In general, the total phase takes the values

$$\theta^{\vec{l}}_j = \beta^{\vec{l}}_j \varphi = \varphi \sum_{k=1}^{j-1} m_k \prod_{i=k+1}^{j-1} (l_i)^{l_i}; \quad \beta \in \mathbb{Z} \tag{20}$$

where $\beta^{\vec{l}}_j$ defines a phase factor of the accumulated phase cycles with phase φ. This excludes filtering for every pair of pathway selection vectors $\vec{l}$ and $\vec{m}$, leading to $\beta = 0$. For every other pathway a filtering can be performed by use of N SPRITE scans with phase cycling steps of

$$\varphi_h = h\frac{2\pi}{N}; \quad h = 1, \ldots, N \tag{21}$$

such that the average over all phase terms φ_h of consecutive scans with the new index h is zero. This means that φ is constant within each scan but varies between consecutive scans. The average over the phase terms of all scans with respect to signal order, j, and transition vector, $\vec{l}$, is given by:

$$\sum_{h=1}^{N} \exp(i\theta^{\vec{l}}_{j,h}) = \langle \exp(i\theta^{\vec{l}}_{j,h}) \rangle_{h=1,\ldots,N} = \left\langle \exp\left(i\beta^{\vec{l}}_j h\frac{2\pi}{N}\right) \right\rangle_{h=1,\ldots,N} = 0 \;\forall\, |\beta| \neq cN; \quad c \in \mathbb{N} \tag{22}$$

Note, that in order to filter the signal of the Nth order FID, N phase-cycled averages need to be taken. In case of two averages $N = 2$, the third order FID for example is not averaged to zero since $\beta = N = 2$ and thus the phase term is always a multiple of 2π. However, these signals are in general small, especially for the small excitation angles that are used in SPRITE. A pictorial description of FID, SE and STE signals for the case of two averages with phase cycling steps of 0° and 180° is shown in Fig. 3. In principle, the quality of the filter improves with the number of averages. Table 1 shows a list of signal components under the influence of one to four phase cycling steps.

2.3. Residual image artefacts

Without averaging, artefacts which can be exactly predicted occur as images with a FOV different to the image from the first order FID. As seen above, the SPRITE data can be interpreted as a superposition of individual k-spaces with different encoding times, t_j.

This leads to a very simple description of the FOV size for the FID images, S^{FID}_j, with signal order, j. The encoding times of the FIDs are simply given by

$$t_j = t_p + (j-1)TR, \quad j = 1, 2, \ldots. \tag{23}$$

where j is the order of the FID. With respect to the gradient step size $\Delta g = \gamma\Delta G/2\pi$, this results in a varying sampling rate in k-space and a changing FOV:

$$\Delta k_j = \Delta g(t_p + (j-1)TR) \tag{24}$$

$$FOV_j = 1/\Delta g(t_p + (j-1)TR) \tag{25}$$

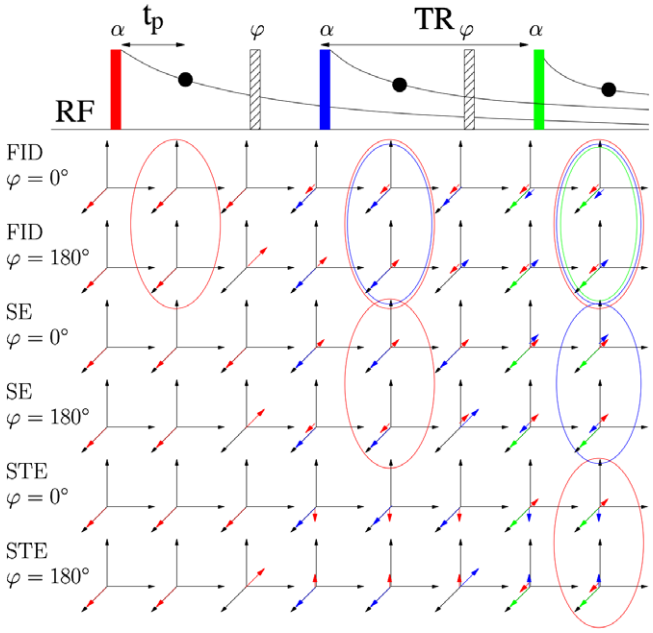

Fig. 3. Signal components of FID, SE, and STE signals are depicted in the reference frame of the local oscillator for phase cycling steps of 0° and 180°. The signals are plotted following three excitation pulses which are colour-coded in red, blue and green. Transverse magnetisation is depicted in the x, y plane and longitudinal magnetisation is vertically oriented in z direction. The signals are shown after excitation, at acquisition and after rotation of the spin system with phase angle $\varphi = 0°, 180°$. The signals excited from ground state are colour-coded with the colour of the related RF excitation pulse. After the second excitation pulse, a shortened vector denotes the relaxation of the signals. The ellipses emphasize signals of interest. The FID signals are always in phase following excitation from ground state. Following the second pulse the FID signals are phase inverted because of phase rotation by phase cycling but are in phase again after the second phase cycling step. SE and STE signals are always acquired with inverted phase.

Table 1
The table shows the effect of the phase cycling filter for signals of first order to fourth order FIDs as well as the spin echo and the stimulated echo with use of one to four averaged scans, N. N also represents the fraction of 2π for the phase cycling steps, φ. The phase factor β is given for all signal components. The averaged signal components are indicated by 0 and non-averaged signal components are denoted by an S.

$\hat{S}_{n,j}$	$\hat{S}^{\mathrm{FID}}_{n,1}$	$\hat{S}^{\mathrm{FID}}_{n,2}$	$\hat{S}^{\mathrm{FID}}_{n,3}$	$\hat{S}^{\mathrm{FID}}_{n,4}$	$\hat{S}^{\mathrm{SE}}_{n,2}$	$\hat{S}^{\mathrm{STE}}_{n,3}$
N	$\beta = 0$	$\beta = 1$	$\beta = 2$	$\beta = 3$	$\beta = 1$	$\beta = 1$
1 $\varphi = 2\pi$	S	S	S	S	S	S
2 $\varphi = \pi$	S	0	S	0	0	0
3 $\varphi = 2\pi/3$	S	0	0	S	0	0
4 $\varphi = \pi/2$	S	0	0	0	0	0

The image points, S_m, are given by the Fourier transformation

$$S^{\mathrm{FID}}_m = \sum_{n=0}^{N-1} \hat{S}^{\mathrm{FID}}_n \exp(i2\pi nm/N) = \sum_{n=0}^{N-1} \sum_{j=1,2,\ldots} \hat{S}^{\mathrm{FID}}_{n,j} \exp(i2\pi \Delta k_j \Delta x_j nm) \quad (26)$$

where

$$\Delta x_j = 1/N\Delta g(t_p + (j-1)TR) \quad (27)$$

defines the voxel size as a function of the order of the FID.

The image is consequently a superposition of images with both reducing voxel volume and signal intensity. In general, only the second order FID contributes significantly to the residual magnetisation since the signal is a function of the cubic voxel volume, Δx^3. Assuming $t_p/TR \sim 1$ and neglecting T_2^* relaxation, the signal per voxel for the second order FID is approximately 10% of the signal of the first order FID. The signal for spin echoes and stimulated echoes would be below 0.7% and 1.5%, respectively, neglecting T_1 and T_2 relaxation and assuming a relatively high flip angle, $\alpha = 10°$. Despite that, spin echo and stimulated echo signals may cause a significant artefact around the centre of the image. The dephasing and rephasing process results in a huge FOV and therefore in a high signal per voxel for stimulated as well as spin echo signals. After the next excitation pulse the transverse magnetisation with pathway selection indices $l = m = 1$ experiences further dephasing. The resulting FOV will be the same as that for the first order FID and may interfere constructively or destructively. Phase cycling cannot filter this signal and that can influence the contrast in such way that quantitative measures of spin density and particularly T_2^* are not reliable. However, this should only be the case if the repetition time, TR, is on the order of, or much shorter than, T_2^*.

Note that in principle, Eqs. (24), (25) and (27) are also valid for standard SPI sequences. In this case, only the repetition time, TR, has to be substituted by the phase encode gradient pulse length, τ, with the assumption of immediate ramp up.

3. Methods

Simulations of the optical transfer functions (OTF), describing a weighting function for the k-spaces and building the Fourier-transform of the point spread function (PSF), was performed using MATLAB 7.0 for a single and a phase cycled SPRITE scan. The transverse and longitudinal relaxation as well as gradient spoiling were taken into account. The assumed relaxation times were $T_2^* = 8.9$ ms and $T_1 = 199$ ms, the repetition time was set to $TR = 8.0$ ms and the encoding time was $t_p = 7.5$ ms. These parameters were chosen for demonstration and comparison with the phantom measurements presented here.

SPRITE proton imaging was performed on a 4 T whole-body scanner with a VARIAN UNITY Inova console using a resolution phantom filled with transformer oil showing two resonance lines separated by 80 Hz. A repetition time, TR, of 8.0 ms was chosen for the SPRITE sequence with a phase encoding time of $t_p = 7.5$ ms per excitation pulse to allow for an increased signal intensity of the second order residual FID acquired at $t_p = 15.5$ ms, with respect to the first order FID. These timing parameters imply also a minimal FOV change of ~2 between the image of the first order FID and the residual image of the second order FID. The FOV was $256 \times 256 \times 256$ mm^3 and a matrix size of $64 \times 64 \times 32$ pixel was acquired. According to the matrix size and the encoding time, the filter bandwidth was set to 11 kHz [10]. Broadband RF pulses with a pulse length of 50 μs and a flip angle of 2° were used to excite the whole volume. Two experiments with 12 averages each were performed. The first series was acquired with phase cycling between 0° and 330° using a phase cycle stepping of 30° whereas the second series was acquired without phase cycling.

4. Results and discussion

Simulation results for a single SPRITE scan and the application of 12 phase-cycled averages are shown in Fig. 4. For repetition times which are short compared to T_2^* a significant residual signal is acquired around the centre of k-space where the self-spoiling property of the phase encode gradients is low. This residual magnetisation gives rise to an incorrect intensity distribution in the reconstructed images. By introducing phase-cycled averaging, the residual magnetisation is efficiently suppressed, and the transient of the longitudinal relaxation becomes the dominant factor in the OTF.

Imaging results are shown in Fig. 5 without the new method (a) and for the phase-cycled average (b). Without phase cycling a residual image appears and the contrast is therefore strongly reduced (Fig. 5a). According to the smaller FOV, and hence a smaller voxel size, the intensity of the residual image should be a factor $(7.5/15.5)^3 \sim 1/8$ smaller than that of the correct image. The ratio of the intensities is only ~1/2 since the two resonances of the transformer oil experience a dephasing phase evolution of about 7.5 ms, and rephasing at about 15.5 ms. The spectrum of the transformer oil (Fig. 6a) shows two distinct lines separated by 80 Hz. According to the line separation, the two resonances cause a re-phasing at ~12.5 ms of the bulk FID (Fig. 6b). Therefore, the residual second order FID acquired at 15.5 ms is of slightly higher intensity than the first order FID acquired at 7.5 ms. Through the use of phase-cycled averaging, the artefacts nearly vanish and the contrast increases significantly (Fig. 5b), as can be seen by comparing the vertical profiles shown in Fig. 7a and b. The signal intensity of the residual image is half that of the image acquired with the phase cycling filter.

The acquired k-space signal is strongly biased by residual magnetisation near the centre. A magnitude profile through the k-space centre in Fig. 7c shows a signal increase by a factor of 2 in the acquisition point immediately following the k-space centre compared to the same profile of the phase-cycled average in Fig. 7d. This is not only because of the short TR but also because of the inefficient spoiling of the transverse magnetisation by the low phase encoding gradient following the k-space centre. The acquired signal of the residual magnetisation follows a different phase encoding and appears as a superimposed image with lower intensity and smaller FOV.

Without the use of a phase cycling filter, the signal intensity and the contrast of the image do not reflect the true T_1-weighted spin density distribution since the acquired k-space strongly deviates from the correct Fourier-transform of the measured object. Therefore, the acquired data are ill suited for spin density measurements and relaxation time mapping. This is even more applicable when

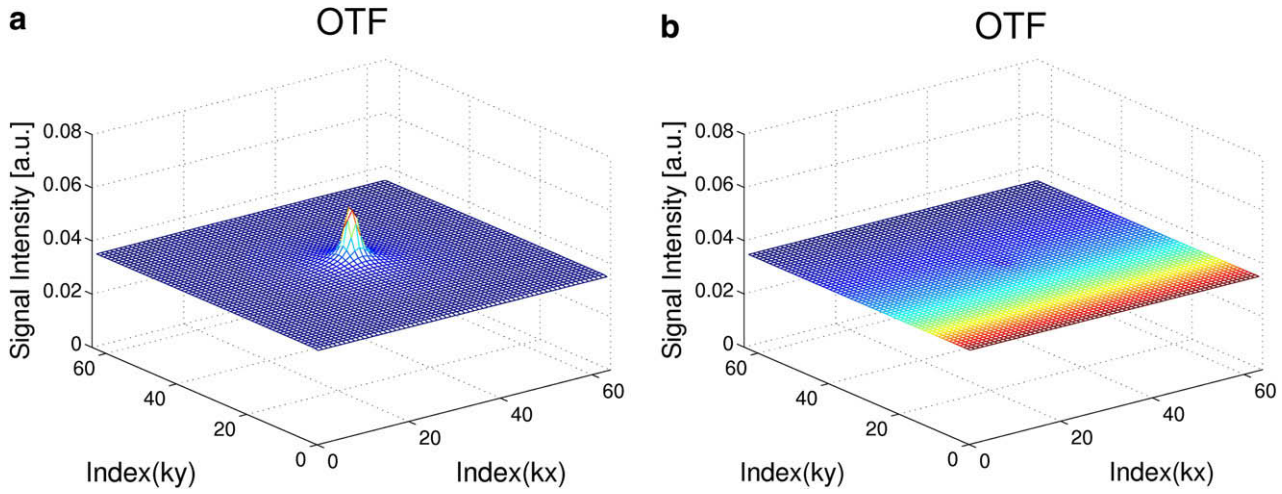

Fig. 4. (a) Simulated OTF of a single SPRITE scan with a short repetition time, TR = 8.0 ms, and encoding time, t_p = 7.5 ms, and relaxation times $T_2^* = 8.9$ ms, T_1 = 199 ms. At the k-space centre a blip caused by the residual magnetisation appears, (b) By averaging 12 phase cycled scans with steps of 30° between 0° and 330° the residual magnetisation vanishes and the transient of longitudinal magnetisation in the direction of the k-space sampling trajectory dominates the OTF. The T_1 transient causes the remaining signal variation.

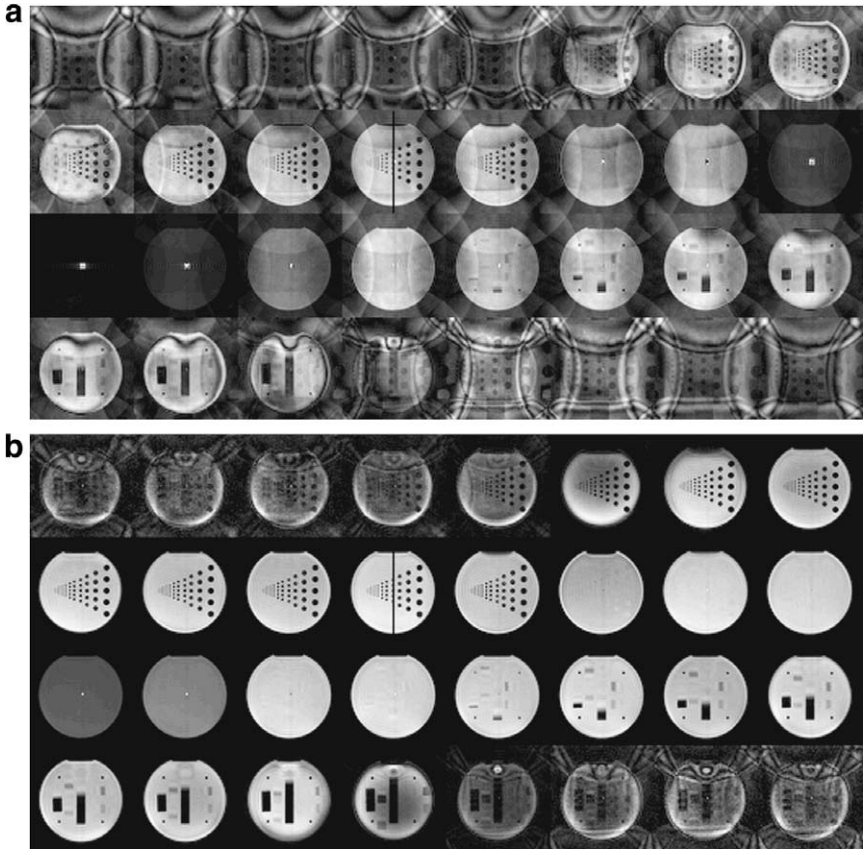

Fig. 5. SPRITE proton imaging results (a) from a single scan and (b) an average of 12 phase cycled scans with phase cycling steps of 0° to 330°. All the acquired 32 slices are presented and each image is scaled separately to maximum (linear grey scale), such that artefacts outside the object are depicted with enhanced intensity. Without phase cycling (a) a pronounced residual image of smaller FOV appears whereas with the proposed phase cycling method (b) the artefact is suppressed efficiently. Note also the Gibbs ringing in the first and last slices outside the phantom which become visible with the use of phase cycling and the DC artefact that is left in the centre slice. The profiles of Fig. 7(a) and (b) are indicated by vertical lines in the fourth slice of the second row.

multiple point acquisition is used, e.g. with the m-SPRITE sequence. Because of different evolution time each image has a different FOV and therefore the signal and the signal relaxation in each voxel of the calculated image series is altered by residual magnetisation of different intensity if a phase cycling filter is not used.

The theoretical framework for the phase-cycled averaging method described here is not tied to the acquisition of single datum points and is generally applicable to the acquisition of echo signals under similar circumstances. Thus, it is reasonable to assume that if TR $\ll T_2$ then the method described here, that of offsetting the frequency of the local oscillator for a short time, τ,

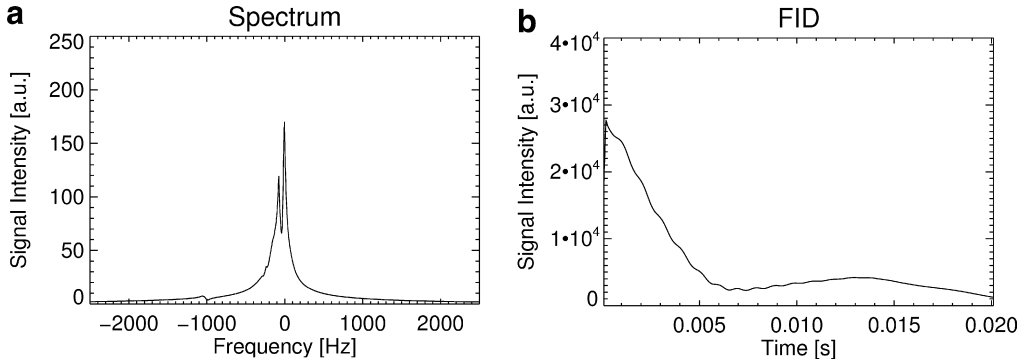

Fig. 6. (a) The spectrum of the transformer oil phantom shows two distinct lines separated by 80 Hz. The highest peak had a line width of 35 Hz related to a transverse relaxation time of $T_2^* = 9$ms. (b) The corresponding bulk FID reflects the phase evolution of the two resonances with rephasing at ~12.5 ms.

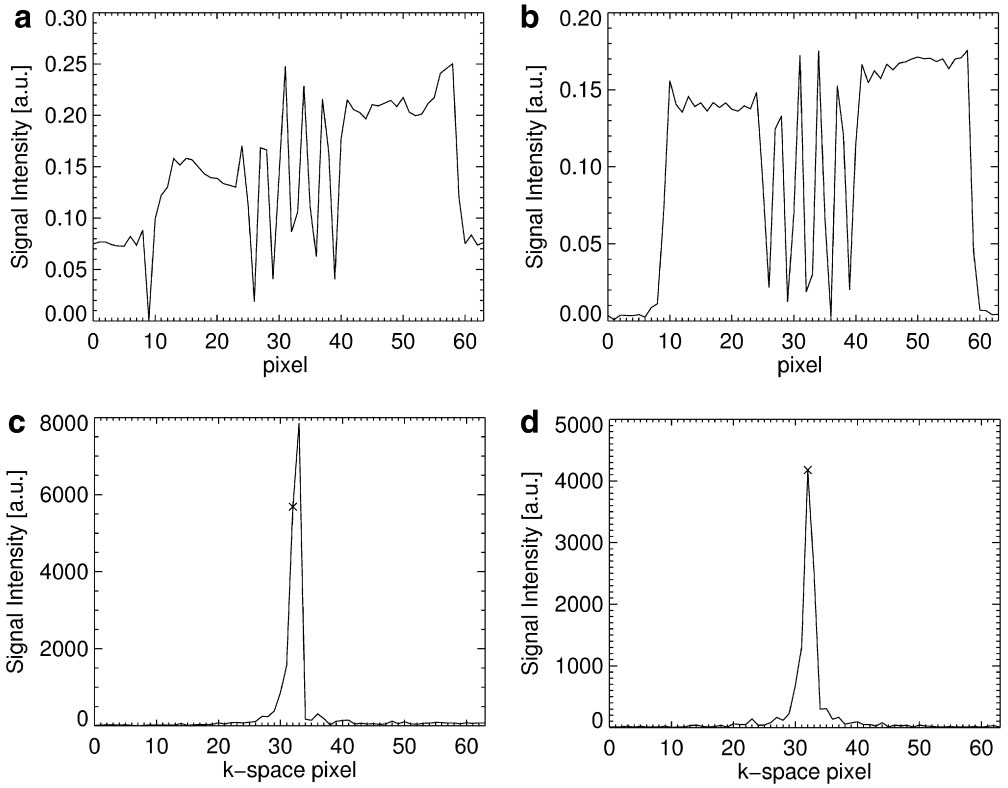

Fig. 7. Vertical profiles through a single slice of the single scan in (a), and with the averaged phase cycled scan (b) (images shown in Fig. 5 (a) and (b), respectively) corresponding to the magnitude profiles through the conjugate data set *k*-space centre in (c) for the single scan and (d) for the averaged phase cycled scan. A cross marks the *k*-space centre in (c) and (d). Significant residual signal appears in the acquisition point following the *k*-space centre as well as the *k*-space centre itself. Both signals experienced no phase encoding due to zero gradients at *k*-space centre acquisition. That is not the case for the acquisition point preceding the *k*-space centre.

with an offset frequency $\Delta\omega$ such that $\varphi = \tau \cdot \Delta\omega$, could also find use in echo imaging.

Recent findings have shown that the increased rate of sodium concentration in the brain after stroke measured with sodium MRI can be used to estimate stroke onset time and could increase the number of subjects who undergo thrombolytic therapy [11]. The quantitative and accurate measurement of tissue sodium concentration is therefore very important to determine disease grade and tissue viability [12]. The SPRITE sequence with the modifications presented in this work is an alternative to the standard methodology for sodium imaging; in terms of its quantitative character and its immunity from artefacts such as blurring effects due to T_2^* decay, for example, SPRITE offers significant advantages for imaging fast-relaxing nuclei. As such, SPRITE with phase cycling may find an increasingly important role in clinical research.

5. Conclusions

Phase-cycled averaging is an easy solution for suppression of the unwanted signal components of residual magnetisation in SPRITE and other SPI sequences. The technique is most efficient for small flip angle excitations. Typically, only small flip angles are used for SPI sequences and therefore, the method is generally applicable. For imaging of nuclei with low SNR, such as sodium, signal averaging is needed in any case, and therefore the method can be used without additional effort in acquisition time. Suppres-

sion of residual magnetisation by phase-cycled averaging is most desirable for quantitative imaging such as spin density and relaxation time mapping.

The method may also be implemented by the use of two RF pulses to acquire two points for averaging separated by a 180° phase cycling module per phase encode gradient step. At least one dummy pulse is needed for the preparation of the residual magnetisation. However, this approach is less efficient since the longitudinal magnetisation is not constant with respect to the two averages and also affects the T_1 weighting of the SPRITE sequence. If acquisition time is critical, SNR is not an issue and spin density or relaxation time mapping are not desired, then this fast phase-cycled averaging may be preferable.

The phase cycling filter has proven to be a highly efficient method for the suppression of residual magnetisation in single point imaging sequences such as SPRITE. The efficiency improves with the number of averages acquired. The presented theory of extended phase encode graphs (EPEG) allows one to understand signal evolution in a SPRITE acquisition in a precise way. The theory predicts the properties of the artefacts introduced by residual magnetisation, correctly, as images of different FOV. It allows for an understanding of the function of the phase cycling method and describes which signals annihilate when averaged.

The use of the phase cycling filter is strongly recommended for use with short repetition times with $TR << T_2^*$. The method will probably be mainly beneficial for the imaging of nuclei with low signal such as sodium.

References

[1] S. Emid, J.H.N. Creyghton, High resolution NMR imaging in solid, Physica B 128 (1985) 81–83.
[2] B.J. Balcom, R.P. MacGregor, S.D. Beyea, D.P. Green, R.L. Armstrong, T.W. Bremner, Single-point ramped imaging with T_1 enhancement (SPRITE), J. Magn. Reson. A 123 (1996) 131–134.
[3] C.B. Kennedy, B.J. Balcom, I.V. Mastikhin, Three-dimensional magnetic resonance imaging of rigid polymeric materials using single-point ramped imaging with T_1 enhancement (SPRITE), Can. J. Chem. 76 (1998) 1753–1765.
[4] E.L. Hahn, Spin echoes, Phys. Rev. 80 (1950) 580.
[5] Z.P. Liang, P.C. Lauterbur, Principles of Magnetic Resonance Imaging, IEEE Press, 1999.
[6] M. Halse, J. Rioux, S. Romanzetti, J.B. Kaffanke, B. MacMillan, I. Mastikhin, N.J. Shah, E. Aubanel, B.J. Balcom, Centric scan SPRITE magnetic resonance imaging: optimization of SNR, resolution, and relaxation time mapping, J. Magn. Reson. 169 (2004) 102–117.
[7] J. Kaffanke, T. Dierkes, S. Romanzetti, M. Halse, J. Rioux, M.O. Leach, B. Balcom, N.J. Shah, Application of chirp z-transform to MRI data, J. Magn. Reson. 178 (2006) 121–128.
[8] R. Kaiser, E. Bartholdi, R.R. Ernst, Diffusion and field-gradient effects in NMR fourier spectroscopy, J. Chem. Phys. 60 (1974) 2966–2979.
[9] D.E. Woessner, Effects of diffusion in nuclear magnetic resonance spin-echo experiments, J. Chem. Phys. 34 (1961) 2057–2061.
[10] S. Gravina, D.G. Cory, Sensitivity and resolution of constant time imaging, J. Magn. Reson. Ser. B 104 (1) (1994) 53–61.
[11] S.C. Jones, A. Kharlamov, B. Yanovski, D.K. Kim, K.A. Easley, V.E. Yushmanov, S.K. Ziolko, F.E. Boada, Stroke onset time using sodium MRI in rat focal cerebral ischemia, Stroke 37 (3) (2006) 883–888.
[12] K.R. Thulborn, D. Davis, J. Snyder, H. Yonas, A. Kassam, Sodium MR imaging of acute and subacute stroke for assessment of tissue viability, Neuroimag. Clin. N Am. 15 (3) (2005) 639–653. xi–xii.